ASPS Conference Proceedings 1: 435-442 (2022)

Proceedings of

12th Structural Engineering Convention - An International Event (SEC 2022)

Available at https://asps-journals.com/index.php/acp

Non-linear Analysis of Axially Loaded Octagonal CFDST Short Columns

R. Manigandan [1, *], Manoj Kumar [2]

[1] Department of Civil Engineering, Research Scholar, Birla Institute of Science and Technology, Rajasthan, 333 031, India
[2]Department of Civil Engineering, Associate Professor, Birla Institute of Science and Technology, Rajasthan, 333 031, India

Paper ID - 040410

Abstract

Concrete Filled Double-skin Steel Tube (CFDST) is a form of composite column that consists of outer steel and an inner steel tube and the space between them is filled with concrete. The structural response of CFDST columns is significantly affected by the thickness of outer and inner steel tubes and the compressive strength of infilled concrete. Although many studies have been in the past to understand the effect of inner and outer tubes thickness on the axial compressive response of circular CFDST columns, no such study appears in the context of octagonal CFDST columns. In this paper, the thickness of both inner and outer tubes is varied. Their effect on axial compressive behavior of CFDST columns containing the concrete of different grades is numerically examined. The non-linear FE analysis of CFDST columns is performed using the ABAQUS. The study shows that axial strength and ductility of octagonal section CFDST columns are significantly influenced by steel tube thickness and the grade of sandwiched concrete. Moreover, the study highlights the importance of the proper selection of inner and outer tube thickness for the better axial response of CFDST columns.

Keywords: CFST, square section, gap, Abaqus, axial load-deformation, Drucker-Prager model

1. Introduction

Concrete Filled Double-skinned Steel Tubes (CFDST) are widely used in high-rise buildings, towers, and bridges owing to lesser weight and greater stiffness [1]. The use of an inner hollow steel tube in a CFDST column reduces the self-weight of the structure and enhances the bending stiffness, ductility, and seismic performance of the column significantly [2]. However, the use of the hollow steel tube in a CFDST column obviously alters the confinement mechanism compared to conventional CFST columns; consequently, the behavior of CFDST columns significantly differs from that of conventional CFST. In the CFDST columns, the confinement mechanism is significantly influenced by the cross-sectional shape, aspect ratio of the section, lateral dimension to thickness ratios of outer and inner steel tubes, and the strength of the materials. The behavior of CFST members is generally found best when they are subjected to axial compression or when the load eccentricity is minimal, implying the loading point is close to the CFST column centroid. As a result, when the CFST member has a high slenderness ratio or is subjected to a large eccentric load, the bending stiffness controls the load-carrying capacity of the column. One cannot take advantage of its excellent compressive strength capacity due to the inadequate bending stiffness of materials near the centroid of the member section. Furthermore, the higher self-weight in conventional CFST columns increases the cost and puts a lot of pressure on the foundations of the structures.

In order to overcome the issues pertaining to CFST columns, the CFDST columns have been utilized and are developing rapidly among researchers and engineers. The CFDST columns are made up of two concentrically joined steel tubes, and the concrete is filled into space between them [3]. Several typical sections used for CFDST columns are shown in Fig. 1. In the last few decades, wide experimental and analytical studies on the structural efficiency of CFDST columns have been performed. Tao [10] conducted the tests on fourteen stub columns having both outer and inner circular hollow sections with different diameter-to-thickness ((D)/(t)) ratios and different hollow section ratios. The experimental observations of these columns proved that the failure mode of the inner tube highly depends upon the D/t ratio, as opposed to that of the outer tube, which was the same for various D/t ratio. Furthermore, the double-skin specimens did not appear to be influenced by the hollow section ratio. Huang [6] analyzed the fourteen specimens identical to those initially introduced by Tao [10] and Hu [32], aiming to investigate the accuracy of modeling using ABAQUS [7]. Based on the study of the axial stress-strain curves for columns, they observed that the columns with a higher confinement factor (ξ) demonstrated strain-hardening behavior, whereas strain-softening behavior was shown for

*Corresponding author. Tel: +919789801266; E-mail address: rmani3830@gmail.com

Published online: December 19, 2022
doi:10.38208/acp.v1.532

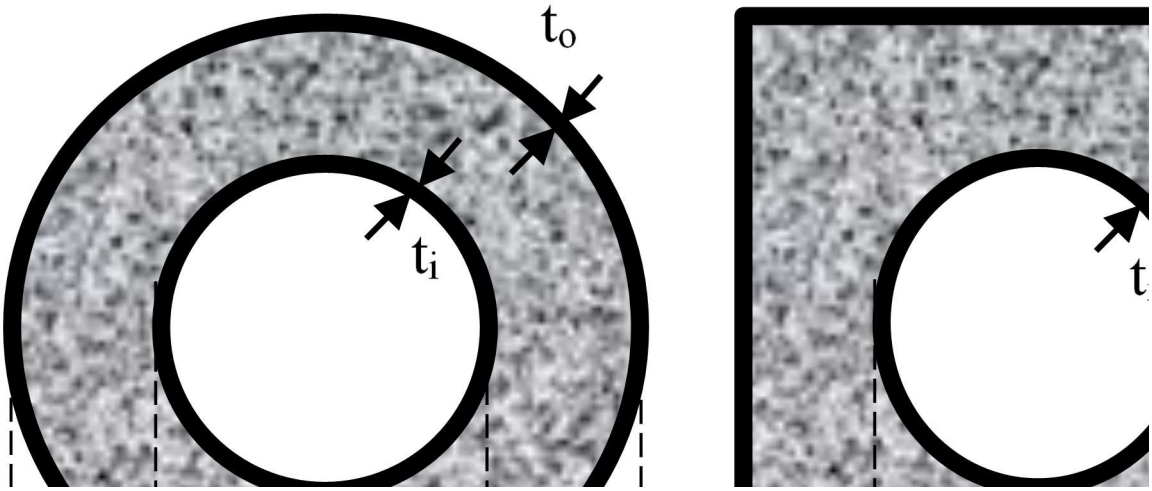

Figure 1 CFDST short columns

smaller ξ values. Elchalakani [8] tested eight specimens with circular outer and square inner skins in the axial compression, and they found that the buckling of both the outer and inner tubes was due to the failure of concrete. In addition, the sections with large slenderness ratios appeared to be more ductile than those with smaller slenderness ratios [9]. than those with smaller slenderness ratios [9]. slenderness ratios appeared to be more ductile than those with smaller slenderness ratios [9].

Aoki [27] investigated the axial load carrying capacity of the polygonal and octagonal CFDST short columns fabricated by welding two half-sections made of folded steel plates. The test results were compared with the plate buckling code in Japan [28] and with the ECCS [29] recommendations for unstiffened circular cylinders. He suggested a design formula to predict the local buckling strength of the polygon CFDST columns. Yang [3] investigated on CFDST column with octagonal outer steel tube and circular inner steel tube under axial compressive load. The test results indicated that the load-bearing capacity of the columns with octagonal section was significantly lower than that of circular section and was higher than that with square section. Godat [11] investigated the performance of polygon CFDST stub columns on local buckling with three different cross-sections: octagonal, dodecagonal, and hendecagonal. Ding [12] investigated the influence of concrete strength and steel ratios on the behavior of octagonal CFDST stub columns under axial compressive

loading in three ways, namely experimentally, numerically, and theoretically. Based on their study, they proposed a simplified design approach. Yang [13] also carried out an experimental and numerical study on the behavior of on octagonal CFDST stub column under axial compression loads. In Yang's study, the CFDST column consisted of an octagonal steel tube as an outer skin tube and a circle of Polyvinyl chloride (PVC) pipe as an inner skin tube, with concrete strength infill between the two layers. He examined the effects of concrete strength, radius to thickness ratio, hollow sectional ratio, and slenderness ratio on the ultimate axial compressive capacity of the CFDST columns. Moreover, he proposed a design formula to predict the ultimate load of the CFDST columns. Alqawzai [14] investigated the octagonal CFDST column under the axial compressive load with and without steel strips. The test result indicated that the CFDST columns with strips performed better than the without strips column.

Although many experimental and analytical studies have been made in the past for different cross-sectional shapes of CFDST columns; however, there are only very few studies on the efficiency of octagonal CFDST short columns under axial compression. Since, in the tubular columns, confinement plays a significant role, and the confinement majorly depends on the cross-sectional shape, it becomes necessary to investigate the axial compressive response of octagonal cross-section CFDST columns. The aim of this study was to investigate the influence of the thicknesses of outer (octagonal) and inner (circular) steel tubes and the strength of sandwiched concrete on the ultimate axial compressive strength of octagonal CFDST short columns. A finite element (FE) analysis was carried out by employing the ABAQUS to predict the behavior of CFDST columns under the axial compressive loads.

2. Finite element modeling

2.1. Modeling of steel

In order to capture the non-linear behavior of steel, a five-stage stress-strain curve has been used, where the stress-strain curve has been divided into five regions, namely, elastic $(O-A)$, elasto-plastic$(A-B)$, plastic $(B-C)$, strain-hardening $(C-D)$ and the secondary plastic $(D-E)$ regions as shown in Fig. 2 [15]. For a steel having yield and ultimate strengths as f_{sy} and f_{su} respectively, the stress-strain relation is assumed linear up to the proportional limit $f_{sp}(=0.8f_{sy})$ and its behavior is considered perfectly plastic when the stress in steel attains the ultimate stress f_{su} $(=1.6f_{sy})$. The stress-strain relation for different regins are as follows:

$\sigma = E_s\varepsilon$ $\quad for\ \varepsilon \le \varepsilon_1$ (=0.8f_{sy}/E_s)

$\sigma = -A\varepsilon^2 + B\varepsilon + C$ $\quad for\ \varepsilon_1 < \varepsilon \le \varepsilon_2$ (=1.5ε_1)

$\sigma = f_{sy}$ $\quad for\ \varepsilon_2 < \varepsilon \le \varepsilon_3 (= 10\varepsilon_2)$

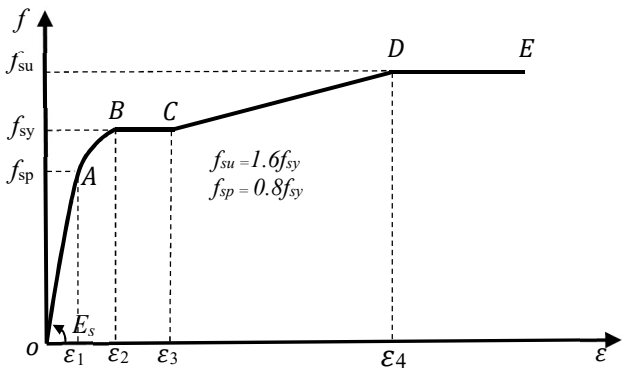

Fig. 2 Stress-strain curve for steel

$$\sigma = f_{sy}\left[1 + 0.6\frac{\varepsilon - \varepsilon_3}{\varepsilon_4 - \varepsilon_3}\right] \quad for\ \varepsilon_3 < \varepsilon \le \varepsilon_4 (= 100\varepsilon_2)$$

$$\sigma = 1.6 f_{sy} \quad for\ \varepsilon > \varepsilon_4$$

where E_s is the modulus of elasticity of steel and A, B and C are constants which are defined as

$$A = \frac{0.2 f_{sy}}{(\varepsilon_2 - \varepsilon_1)^2}, B = 2A\varepsilon_2, \qquad C = 0.8 f_{sy} + A\varepsilon_1^2 - B\varepsilon_1$$

where, $\varepsilon_1 = 0.8 f_{sy}/E_s$ and $\varepsilon_2 = 1.5\ \varepsilon_1$

2.1 Modeling of Concrete Core

Various researchers have proposed several stress-strain models to define stress variation with strain in the confined concrete [16–19]. The uniaxial stress-strain model proposed by Hu [20] has been proved to predict the behavior of concrete confined in steel tubes satisfactorily, and it is widely used to analyze the CFST and CFDST columns [21–24]; the same has been adopted in this study. In the stress-strain model proposed by Hu [20], the enhanced peak compressive strength of confined concrete (f'_{cc}) due to lateral confining pressure (f_l) and the peak strain (ε'_{cc}) corresponding to f'_{cc} are defined as

$$f'_{cc} = f_c + k_1 f_l$$
$$\varepsilon'_{cc} = \varepsilon'_c\left[1 + k_2\ \frac{f_l}{f'_c}\right]$$

Where f'_c is the uni-axial unconfined cylindrical compressive strength of concrete, ε'_c is the peak strain corresponding to stress f'_c which is usually considered 0.002 as specified by ACI [30]. In Eqs. 2 and 3, k_1 and k_2 are constants and they are recommended by Richart [25] as 4.1 and 20.5, respectively. In CFDST columns, the magnitude of f_l significantly depends on the cross-sectional shape and the lateral dimension to steel tube thickness ratio. According to Hu [31], the magnitude of lateral confining pressure f_l for octagonal CFDST column can be determined using the following equations.

$$f_l = 8.525 - 0.166\left(\frac{D_0}{t_0}\right) - 0.00897\left(\frac{d_i}{t_i}\right) + 0.00125\left(\frac{D_0}{t_0}\right)^2 + 0.00246\left(\frac{D_0}{t_0}\right)\times\left(\frac{d_i}{t_i}\right) - 0.00550\left(\frac{d_i}{t_i}\right)^2 \ge 0 \quad (4)$$

$$\frac{f_l}{f_{yi}} = 0.01844 - 0.00055\left(\frac{D_0}{t_0}\right) - 0.00040\left(\frac{d_i}{t_i}\right) + 0.00001\left(\frac{D_0}{t_0}\right)^2 + 0.00001\left(\frac{D_0}{t_0}\right)\times\left(\frac{d_i}{t_i}\right) - 0.00002\left(\frac{d_i}{t_i}\right)^2 \quad (5)$$

$$\frac{f_l}{f_{yo}} = 0.01791 - 0.00036\left(\frac{D_0}{t_0}\right) - 0.00013\left(\frac{d_i}{t_i}\right) + 0.00001\left(\frac{D_0}{t_0}\right)^2 + 0.00001\left(\frac{D_0}{t_0}\right)\times\left(\frac{d_i}{t_i}\right) - 0.00002\left(\frac{d_i}{t_i}\right)^2 \quad (6)$$

where f_y = yield strength of the steel tube, D_o = distance between the parallel sides of external octagonal steel tube, d_i = diameter of the internal steel tube, and t_0 , t_i = thickness of outer and inner steel tubes, respectively.

Hu [20] suggested that the stress-strain relation for confined concrete may be considered a combination of a parabolic segment from A to B and a descending straight-line segment from B to C as shown in Fig. 3. In the parabolic segment, the stress (f) corresponding to strain (ε) is expressed as

$$f = \frac{E_c\varepsilon}{1+(R+R_E-2)\left[\frac{\varepsilon'_c}{\varepsilon'_{cc}}\right]-(2R-1)\left[\frac{\varepsilon'_c}{\varepsilon'_{cc}}\right]^2+R\left[\frac{\varepsilon'_c}{\varepsilon'_{cc}}\right]^3} \quad (7)$$

where, E_{cc} is the modulus of elasticity of confined concrete, and its value may be calculated using the recommendations of ACI [30] as

$$E_c = 4700\sqrt{f'_{cc}} \quad (8)$$

In eq. 4, R and R_E are the model parameters and they are defined as (Hu *et al.* 2003)

$$R = \frac{R_E(R_\sigma - 1)}{(R_\varepsilon - 1)^2} - \frac{1}{R_E}\ ;\ R_E = \frac{E_c\,\varepsilon'_{cc}}{f'_{cc}};\ R_\varepsilon = R_\sigma = 4 \quad (9)$$

In the descending segment of the stress-strain curve, stress is assumed to decrease from peak stress linearly (f'_{cc}) up to the stress at the ultimate stage. Hu [20] recommended the magnitude of ultimate strain (ε_u) and ultimate stress (f_u) as $11\varepsilon'_{cc}$ and $K_3 f'_{cc}$ respectively, where K_3 is a parameter, and its value depends on the cross-sectional shape and the lateral cross-sectional dimension to steel tube thickness ratio. The value of K_3 for octagonal CFDST columns is calculated using the following empirical relations [31].

$$k_3 = 1.73916 - 0.00862\left(\frac{D_0}{t_0}\right) - 0.04731\left(\frac{d_i}{t_i}\right) + 0.00036\left(\frac{D_0}{t_0}\right)^2 + 0.00134\left(\frac{D_0}{t_0}\right)\times\left(\frac{d_i}{t_i}\right) - 0.00058\left(\frac{d_i}{t_i}\right)^2 \ge 0 \quad (10)$$

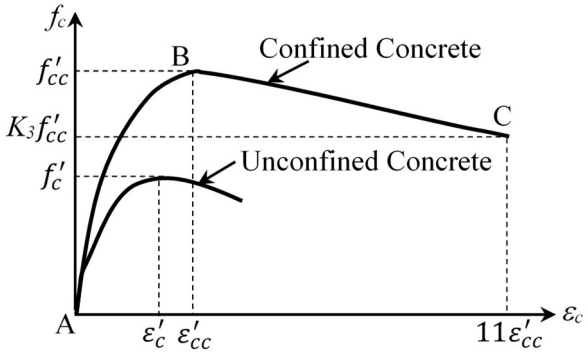

Fig. 3. Stress-Strain Curve of Confined

2.3 Finite Element Discretization

In the CFDST column, the concrete and the inner and outer steel tubes are modeled using the 8-node brick elements with reduced integration (C3D8R) [26]. The finite element meshes for the typical member with circular, square, and octagonal sections are shown in Fig. 4. For the application of boundary conditions and axial load on CFDST columns in ABAQUS, the reference points RP1 and RP2 were considered at the top and bottom face of the column. All the nodes of the concrete core and both the steel tubes located at the top face of the column were connected to RP1 via rigid ties, and similarly, all the nodes of the concrete core and steel tubes located at the bottom face were connected to RP2. While determining the columns axial compressive strength via experiments, normally rigid steel plates are provided at the top, and bottom face of the column and these plates restrain the rotations at the ends of the column. In order to replicate the boundary conditions analogous to those experienced by CFDST during the experiment, the RP2 was fully restrained $\left(\boldsymbol{i.e.}\, \boldsymbol{U_x = U_y = U_z = UR_x = UR_y = UR_z = 0}\right)$ while the point RP1 was allowed to displace along axial loading direction only $\left(\boldsymbol{i.e.}\; \boldsymbol{U_x = U_y = UR_x = UR_y = UR_z = 0};\; \boldsymbol{U_z \neq 0}\right)$ as shown in Fig. 7. The axial load was applied at RP1 concentrically in the form of displacement control. For the simulation of plastic deformation in the concrete core, the Extended Drucker-Pager model [7] was used, and the parameters associated with this model given as input in ABAQUS were Angle of friction, ϕ = 20°, Flow Stress ratio, k = 0.8, and Dilation angle, β = 20° [20].

2.4 Modeling of interaction between steel tube and concrete

To simulate the interaction between the steel tube and concrete in the CFDST column, the contact interaction, available in ABAQUS [7], has been used in the present study. In ABAQUS, the contact interaction is expressed in terms of geometric and mechanical properties. For defining the

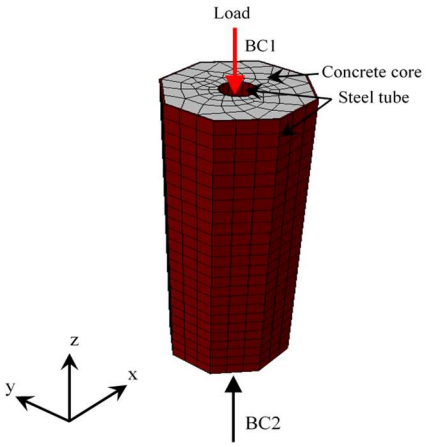

BC1(RP-1): Clamped boundary condition $\left(U_x = U_y = UR_x = UR_y = UR_z = 0;\; U_z \neq 0\right)$
BC2 (RP-2): Fixed boundary condition $\left(U_x = U_y = U_z = UR_x = UR_y = UR_z = 0\right)$

Fig. 4. Schematic view of mesh configurations and boundary conditions

geometrical property of contact surfaces, firstly, an appropriate contact discretization is considered; subsequently, master and slave surfaces are identified. In this study, steel is considered master surface, and concrete is defined as slave surface, allowing the penetration of the steel tube in concrete, but the reverse is not permitted. However, in CFDST columns, such penetrations can be further eliminated by carefully selecting the master surface and discretizing contact surfaces with the finite elements [6].

Moreover, a small sliding tracking approach is selected for the contact. Since the actual sliding between steel and concrete surfaces in the CFDST column would be relatively minimal, this method is more effective in the calculation. The precision of the finite element modeling was verified by developing FE models and comparing them with the results of preceding experiments.

3. Validation of the FE model

Validation of the current models involved a comparison of previous experimental results of Alqawzai [14] and Yang [3] with the corresponding ABAQUS model considering both concrete and steel models are given above. The geometric details and material properties of a total of 5 analyzed specimens, along with their experimental, are shown in Table 1. where $\boldsymbol{N_{u,Exp}}$ is the experimental compressive strength and $\boldsymbol{N_{u,FEM}}$ presents the ultimate axial load predicted by the non-linear FE analysis. The axial load vs. axial shortening behavior of the CFDST specimens, namely O1S00, 02S00, are shown in Fig.5. The figure

Table 1. Validation of numerical modeling to predict the ultimate axial compressive strength of octagonal CFDST column.

Specimens	D_o (mm)	t_o (mm)	d_i (mm)	t_i (mm)	L (mm)	f_{syo} (MPa)	f_{syi} (MPa)	f'_c (MPa)	$N_{u,Exp}$ (kN)	$N_{u,FEM}$ (kN)	$\frac{N_{u,FEM}}{N_{u,Exp}}$	Ref
O1S00	300	2.7	114	4	900	468.3	437.3	42.5	3139	3207	1.02	[12]
O2S00	300	2.7	180	5	900	468.3	375.5	38.4	3130	3119	1.00	
2	197	3.3	108	3	594	300.0	260.0	37.0	1904	2011	1.06	
3	216	3.4	108	3	648	300.0	260.0	37.0	2461	2498	1.02	[3]
4	240	3.3	114	3	720	300.0	365.0	37.0	2996	3223	1.08	

Table 2. Effect of outer and inner steel tube thickness and concrete strength on ultimate axial load Strength of octagonal CFDST Columns

Spec. No	D_o (mm)	t_o (mm)	$\frac{D_o}{t_o}$	d_i (mm)	t_i (mm)	$\frac{d_i}{t_i}$	L (mm)	f_{syo}, f_{syi} (MPa)	f_c (MPa)	$N_{u,FEM}$ (kN)	$N_{u,EC4}$ (kN)
OC–O1	379	3.0	126	100	3.0	33	900	345	51	5007	5283
OC–O2	379	3.5	108	100	3.0	33	900	345	51	5332	5473
OC–O3	379	4.0	95	100	3.0	33	900	345	51	5492	5662
OC–O4	379	4.5	84	100	3.0	33	900	345	51	5561	5885
OC–O5	379	5.0	76	100	3.0	33	900	345	51	5713	6044
OC–I1	379	3.0	126	100	3.5	29	900	345	51	5321	5333
OC–I2	379	3.0	126	100	4.0	25	900	345	51	5404	5383
OC–I3	379	3.0	126	100	4.5	22	900	345	51	5489	5433
OC–I4	379	3.0	126	100	5.0	20	900	345	51	5545	5482
OC–CS1	379	3.0	126	100	3.0	33	900	345	35	4903	4130
OC–CS2	379	3.0	126	100	3.0	33	900	345	55	6415	5571
OC–CS3	379	3.0	126	100	3.0	33	900	345	75	7621	7012
OC–CS4	379	3.0	126	100	3.0	33	900	345	95	8324	8453
OC–CS5	379	3.0	126	100	3.0	33	900	345	105	9219	9173

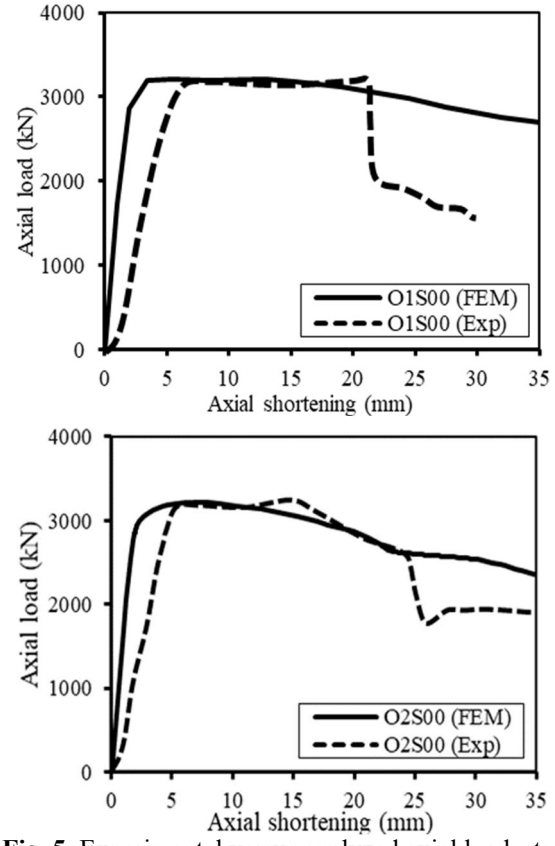

Fig. 5. Experimental versus analyzed axial load–strain curves for specimens O1S00 and O2S00.

demonstrates the post-peak behavior and the ultimate load of the octagonal CFDST column. However, the numerical model exhibited superior ductility to its experimental counterpart. Furthermore, the specimen displayed an equal axial load vs. axial shortening performance until the experimental column reached its maximum capacity. The model shows better behavior in terms of its ultimate strength and post-peak (ductility).

Moreover, Table 2 shows that with the increase in outer steel tube thickness from 3 mm to 5 mm, the (D_o/t_o) ratio reduces from 126 to 76; as a result, the axial load carrying capacity of the column increases by 14%, mainly because of an increase in the outer steel tube cross-section area.

4.1 Effects of (d_i/t_i) ratio on Compressive Response of CFDST Columns

To examine the influence of the (d_i/t_i) ratio on the compressive response of CFDST columns, keeping the diameter of the inner steel tube (d_i) constant, the thickness of the inner tube was varied from 3 mm to 5 mm. The axial compressive strengths of OC-I1 to OC-I4 column specimens with different inner tube thicknesses are listed in Table 2, and the axial load-displacement curves for these columns are shown in Fig. 6 (b). Table 2 depicts that the (d_i/t_i) ratio has little effect on the ultimate axial compressive strength of columns. This could be because the contribution of the inner steel tube in steel provided in the column is smaller than the outer steel tube. The study reveals that the thickness of the inner steel tube may be selected smaller to reduce the self-weight of the column as well to reduce the cost of the structure.

4.1 Effects of concrete compressive strength (f_c)

The octagonal CFDST columns were analyzed with different cylindrical compressive strengths of concrete ranging between 35 to 105 MPa at an interval of 20 MPa. The compressive strengths of OC-CS1 to CS5 columns with different concrete strengths are shown in Table 2, and the axial load-deformation curves for these columns are shown in Fig. 6 (c). The table shows that the axial compressive strength of the column enhances with the increase in the cylindrical compressive strength of concrete. Moreover, the Table exhibits that while increasing the concrete strength from 35 MPa to 105 MPa, the axial compressive strength of the column increases by 88%. Moreover, Fig. 5 (c) shows that the axial load-displacement curves of the columns tend to show similar load-deformation responses, and the trend of the load-deformation remains almost unaltered up to the failure stage.

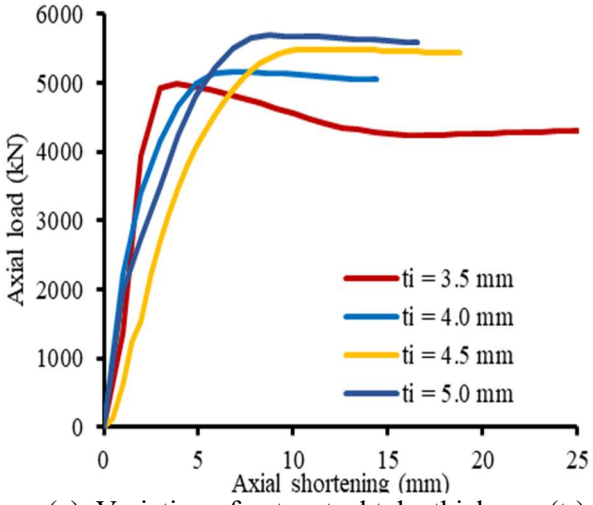

(a) Variation of outer steel tube thickness (t_o)

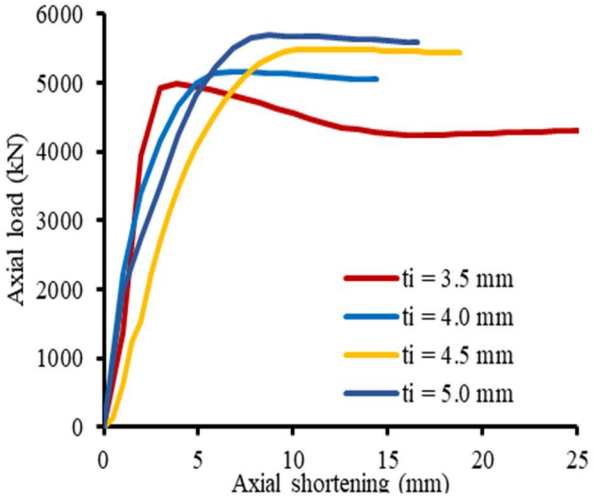

(b) Variation of inner steel tube thickness (t_i)

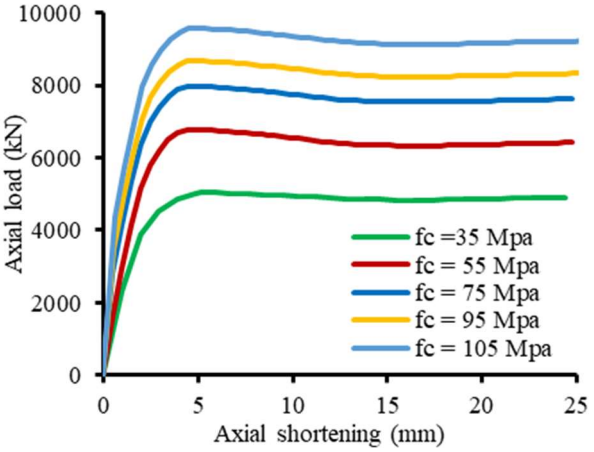

(c) Variation of Different Concrete Strength (f_c)

Fig. 6. Axial Load-axial deformation response of octagonal CFDST columns having (a) Variation of outer steel tube thickness [t_o], (b) Variation of inner steel tube thickness [t_i], and (c) Variation of Different Concrete Strength [f_c]

4.2 Compressive strength of CFDST columns according to Eurocode-4

In order to check the feasibility of using the Eurocode-4 (EC4) procedure for calculating the axial compressive strength of octagonal CFDST columns, the numerically determined axial compressive strength of octagonal CFDST columns are compared with those calculated according to EC4 as shown in Table 2. In this study, the (D_o/t_o) and (d_i/t_i) ratios of the column are varied between 126 to76 and 33 to 20, respectively Moreover, keeping the (D_o/t_o) and (d_i/t_i) ratio fixed as 126 and 33 respectively, the cylindrical strength of concrete is varied from 35 to 105 MPa. Table 2 indicates that for the medium concrete strength (51 MPa) and smaller internal tube thickness (3 mm and 3.5 mm), the EC4 overestimates the axial compressive strength of octagonal columns; however, as the thickness of the internal tube is gradually increased from 3.5 mm to 5 mm, the EC4 tends to underestimate the compressive of the column. Moreover, for the CFDST columns having internal and outer steel tube thicknesses equal to 3 mm, as the concrete strength is increased from 35 to 75 MPa, the EC4 underestimates the compressive of CFDST column, and for higher concrete strengths (95 and 105 MPa), the EC4 again overestimates the compressive strengths. Hence, for the normal strength concrete (51 MPa), EC4 may safely be used to calculate the axial strength of octagonal CFDST columns having the (D_o/t_o) and (d_i/t_i) ratios between 126 to 76 and 33 to 28, respectively.

5 Conclusions

The aim of this paper was to evaluate the influence of the thicknesses of outer (octagonal) and inner (circular) steel tubes and the strength of sandwiched concrete on the ultimate axial compressive strength of concrete-filled double-skinned tubular (CFDST) short columns. A finite element (FE) analysis was carried out by employing the ABAQUS to predict the behavior of CFDST columns under the axial compressive loads. Based on the numerical results, the following conclusions have been drawn

- The finite element method is capable to numerically simulate the complex behavior of composite CFDST columns.
- The axial compressive strength of octagonal CFDST column specimens significantly decreases as the outer width to thickness ratio i.e. (D_o/t_o) increases, however, the inner tube diameter to thickness ratio i.e. (d_i/t_i) seems to have less effect on the compressive strength.
- The strength of sandwiched concrete is observed to highly influence the axial compressive strength of the CFDST columns.
- The Eurocode-4 may safely be used to determine the axial compressive strength of octagonal CFDST columns having the (D_o/t_o) and (d_i/t_i) ratios between 126 to 76 and 33 to 20, respectively.

Disclosures

Free Access to this article is sponsored by SARL ALPHA CRISTO INDUSTRIAL.

References

1. Pagoulatou M, Sheehan T, Dai XH, Lam D. Finite element analysis on the capacity of circular concrete-filled double-skin steel tubular (CFDST) stub columns. Engineering Structures (2014) 72: 102–12. https://doi.org/10.1016/j.engstruct.2014.04.039.

2. Ho JCM, Dong CX. Improving strength, stiffness and ductility of CFDST columns by external confinement. Thin-Walled Structures (2014) 75: 18–29. https://doi.org/10.1016/j.tws.2013.10.009.

3. Yang J, Xu H, Peng G. Behavior of concrete-filled double skin steel tubular columns with octagon section under axial compression. Frontiers of Architecture and Civil Engineering in China (2008) 2: 205–10. https://doi.org/10.1007/s11709-008-0035-5.

4. Huang H, Han LH, Tao Z, Zhao XL. Analytical behaviour of concrete-filled double skin steel tubular (CFDST) stub columns. Journal of Constructional Steel Research (2010) 66: 542–55. https://doi.org/10.1016/j.jcsr.2009.09.014.

5. ABAQUS (2014). Analysis user's manual 6.14-EF, Dassault Systems Simulia Corp., Providence.

6. Elchalakani M, Zhao XL, Grzebieta R. Tests on concrete filled double-skin (CHS outer and SHS inner) composite short columns under axial compression. Thin-Walled Structures (2002) 40:415–41. https://doi.org/10.1016/S0263-8231(02)00009-5.

7. Zhao X-L, Grzebieta R, Elchalakani M. Tests of concrete-filled double skin CHS composite stub columns. Steel and Composite Structures (2002) 2: 129–46. https://doi.org/10.12989/scs.2002.2.2.129.

8. Han L-H, Zhao X-L, Tao Z. Tests and mechanics model for concrete-filled SHS stub columns, columns and beam-columns. Steel and Composite Structures (2001) 1: 51–74. https://doi.org/10.12989/scs.2001.1.1.051.

9. Godat A, Legeron F, Bazonga D. Stability investigation of local buckling behavior of tubular polygon columns under concentric compression. Thin-Walled Structures (2012) 53: 131–40. https://doi.org/10.1016/j.tws.2011.12.013.

10. Ding FX, Fang C, Bai Y, Gong YZ. Mechanical performance of stirrup-confined concrete-filled steel tubular stub columns under axial loading. Journal of Constructional Steel Research (2014) 98: 146–57. https://doi.org/10.1016/j.jcsr.2014.03.005.

11. Yuan W Bin, Yang JJ. Experimental and numerical studies of short concrete-filled double skin composite tube columns under axially compressive loads. Journal of Constructional Steel Research (2013) 80: 23–31. https://doi.org/10.1016/j.jcsr.2012.09.014.

12. Alqawzai S, Chen K, Shen L, Ding M, Yang B, Elchalakani M. Behavior of octagonal concrete-filled double-skin steel tube stub columns under axial compression. Journal of Constructional Steel Research (2020) 170: 106115. https://doi.org/10.1016/j.jcsr.2020.106115.

13. Han LH, Yao GH, Zhao XL. Tests and calculations for hollow structural steel (HSS) stub columns filled with self-consolidating concrete (SCC). Journal of Constructional Steel Research (2005) 61: 1241–69. https://doi.org/10.1016/j.jcsr.2005.01.004.

14. Karthik MM, Mander JB. Stress-Block Parameters for Unconfined and Confined Concrete Based on a Unified Stress-Strain Model. Journal of Structural Engineering (2011) 137: 270 -3. https://doi.org/10.1061/(asce)st.1943-541x.0000294.

15. Carreira, D.J.; Chu, K.D. Stress-Strain Relationship for Plain Concrete in Compression. ACI Structural Journal (1985) :797–804.

16. Mansur MA, Wee TH, Chin MS. Derivation of the complete stress-strain curves for concrete in compression. Magazine of Concrete Research (1995) 47: 285–90. https://doi.org/10.1680/macr.1995.47.173.285.

17. Lai MH, Ho JCM. A theoretical axial stress-strain model for circular concrete-filled-steel-tube columns. Engineering Structures (2016) 125: 124–43. https://doi.org/10.1016/j.engstruct.2016.06.048.

18. Hu HT, Huang CS, Wu MH, Wu YM. Non-linear analysis of axially loaded concrete-filled tube columns with confinement effect. Journal of Structural Engineering (2003) 129: 1322–9. https://doi.org/10.1061/(ASCE)0733-9445(2003)129:10(1322).

19. Liao FY, Han LH, Tao Z. Behaviour of CFST stub columns with initial concrete imperfection: Analysis and calculations. Thin-Walled Structures (2013) 70: 57–69. https://doi.org/10.1016/j.tws.2013.04.012.

20. Han LH, Yao GH, Tao Z. Performance of concrete-filled thin-walled steel tubes under pure torsion. Thin-Walled Structures (2007) 45: 24–36. https://doi.org/10.1016/j.tws.2007.01.008.

21. Chen J, Wang J, Xie F, Jin WL. Behavior of thin-walled dodecagonal section double skin concrete-filled steel tubes under bending. Thin-Walled Structures (2016) 98: 293–300. https://doi.org/10.1016/j.tws.2015.10.002.

22. Ci J, Jia H, Ahmed M, Chen S, Zhou D, Hou L. Experimental and numerical analysis of circular concrete-filled double steel tubular stub columns with inner square hollow section. Engineering Structures (2021) 227: 111400. https://doi.org/10.1016/j.engstruct.2020.111400.

23. Richart FE, Brandtzaeg A, Brown RL. A study of the failure of concrete under combined compressive stresses. Bulletin No 185 Engineering Experiment Station (1928) 26: 7–92.

24. Albero V, Ibañez C, Piquer A, Hernández-Figueiredo D. Behaviour of slender concrete-filled dual steel tubular columns subjected to eccentric loads. Journal of Constructional Steel Research (2021) 176. https://doi.org/10.1016/j.jcsr.2020.106365.

25. Aoki, T., Migita, and Y. Fukumoto. Local buckling strength of closed polygon folded section columns. Journal of Constructional Steel Research (1991) 20 (4): 259–270. https://doi.org/10. 1016/0143-974X(91)90077-E.

26. Japan Highway Association, Specification for Highway Bridges (Steel Bridge), (1980).

27. European Recommendations for Steel Construction, Buckling of Shells ECCS-CECMEKS, (1983) 7.

28. ACI Committee 318. Building code requirements for structural concrete and commentary (ACI 318-08). Detroit, Michigan: American Concrete Institute; 2014.

29. Hu HT, Su F. Nonlinear analysis of short concrete-filled double skin tube columns subjected to axial compressive forces. Marine Structures, (2011) (24):319–337.

30. Huang CS, Yeh Y-K, Liu G-Y, Hu H-T, Tsai KC, Weng YT, et al. Axial Load Behavior of Stiffened Concrete-Filled Steel Columns. Journal of Structural Engineering (2002) (128): 1222–30. https://doi.org/10.1061/(asce)0733-9445(2002)128:9(1222).